Molecular Microbiology (2016) 00(00), 00–00

doi:10.1111/mmi.13605
First published online 2016

Structural mechanism for bacterial oxidation of oceanic trimethylamine into trimethylamine *N*-oxide

Chun-Yang Li,[1] Xiu-Lan Chen,[1] Dian Zhang,[1] Peng Wang,[1] Qi Sheng,[1] Ming Peng,[1] Bin-Bin Xie,[1] Qi-Long Qin,[1] Ping-Yi Li,[1] Xi-Ying Zhang,[1] Hai-Nan Su,[1] Xiao-Yan Song,[1] Mei Shi,[1] Bai-Cheng Zhou,[1] Lu-Ying Xun,[1] Yin Chen[2] and Yu-Zhong Zhang[1,3]*

[1]*State Key Laboratory of Microbial Technology, Marine Biotechnology Research Center, Institute of Marine Science and Technology, Shandong University, Jinan 250100, China.*

[2]*School of Life Sciences, University of Warwick, Coventry CV4 7AL, UK.*

[3]*Laboratory for Marine Biology and Biotechnology, Qingdao National Laboratory for Marine Science and Technology, Qingdao, China.*

Summary

Trimethylamine (TMA) and trimethylamine *N*-oxide (TMAO) are widespread in the ocean and are important nitrogen source for bacteria. TMA monooxygenase (Tmm), a bacterial flavin-containing monooxygenase (FMO), is found widespread in marine bacteria and is responsible for converting TMA to TMAO. However, the molecular mechanism of TMA oxygenation by Tmm has not been explained. Here, we determined the crystal structures of two reaction intermediates of a marine bacterial Tmm (*Rn*Tmm) and elucidated the catalytic mechanism of TMA oxidation by *Rn*Tmm. The catalytic process of Tmm consists of a reductive half-reaction and an oxidative half-reaction. In the reductive half-reaction, FAD is reduced and a C4a-hydroperoxyflavin intermediate forms. In the oxidative half-reaction, this intermediate attracts TMA through electronic interactions. After TMA binding, $NADP^+$ bends and interacts with D317, shutting off the entrance to create a protected micro-environment for catalysis and exposing C4a-hydroperoxyflavin to TMA for oxidation. Sequence analysis suggests that the proposed catalytic mechanism is common for bacterial Tmms. These findings reveal the catalytic process of TMA oxidation by marine bacterial Tmm and first show that $NADP^+$ undergoes a conformational change in the oxidative half-reaction of FMOs.

Accepted 6 December, 2016. *For correspondence. E-mail zhangyz@sdu.edu.cn; Tel. +86 531 88564326; Fax +86 531 88564326.

Introduction

Methylated amines (MAs), such as trimethylamine (TMA) and trimethylamine *N*-oxide (TMAO), are ubiquitous in marine environments, and represent a significant pool of carbon and nitrogen in the ocean (Gibb and Hatton, 2004; Chen *et al*., 2011; Carpenter *et al*., 2012). Volatile MAs are precursors of nitrous oxide (a greenhouse gas) in marine atmospheres and marine aerosols (Quinn *et al*., 1988; Carpenter *et al*., 2012). TMAO plays important roles in many physiological processes (Seibel and Walsh, 2002). For example, TMAO acts as a potent protein stabilizer in deep-sea organisms (Ma *et al*., 2014; Yancey *et al*., 2014). TMAO can also act as an electron acceptor for anaerobic respiration (Arata *et al*., 1992; Gon *et al*., 2001).

Flavin-containing monooxygenases (FMOs) and cytochrome P450 are two effective families involved in the metabolism of xenobiotics in eukaryotes. FMOs belong to the class B of flavoprotein monooxygenases and can oxygenate a wide range of substrates, such as nitrogen-containing and sulfur-containing compounds (Van Berkel *et al*., 2006). FMOs have been well studied in eukaryotes, including plants, fungi and mammals (Cashman, 1995; Suh *et al*., 1999; Suh and Robertus, 2000; Krueger and Williams, 2005; Koch *et al*., 2006; Schlaich, 2007). Notably, there are five functional FMO isoforms in human (Cashman and Zhang, 2006), and some mutations in isoform 3 of human FMO (hFMO3) can cause an inheritable disease, trimethylaminuria (TMAU), also known as “fish-odor syndrome” (Mitchell and Smith, 2001; Zhou and Shephard, 2006).

Bacterial FMOs homologous to hFMO3 oxidize TMA to TMAO (Choi *et al*., 2003; Chen *et al*., 2011), and they are TMA monooxygenases (Tmms) (Chen *et al*., 2011). Physiological analysis suggests that Tmms are essential for bacteria to utilize TMA as a nitrogen source

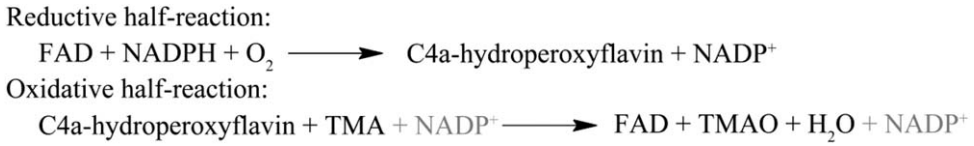

Fig. 1. The reaction scheme for TMA oxidation by Tmm. The catalytic process of Tmm can be divided into a reductive half-reaction and a followed oxidative half-reaction. In the oxidative half-reaction, $NADP^+$ is colored in gray because its function is controversial.

(Chen *et al*., 2011). The *tmm* gene is found highly abundant in the metagenomes of the Global Ocean Sampling data set, particularly in marine *Roseobacter* clade (MRC) and the SAR11 clade, which are both abundant in marine environments and are important participants in marine C, S and N cycles (Morris *et al*., 2002; Buchan *et al*., 2005; Rusch *et al*., 2007; Chen *et al*., 2011; Chen, 2012). It is estimated that approximately 20% of bacteria in the surface ocean contain *tmm* (Chen *et al*., 2011), suggesting that Tmm plays an important role in marine N and C cycles. However, the molecular mechanism of Tmm to oxidize TMA to TMAO still remains unclear.

Tmm is able to catalyze oxygenations on a wide range of substrates, such as TMA, indole and methimazole (Alfieri *et al*., 2008; Orru *et al*., 2010; Cho *et al*., 2011). The catalytic process of Tmm to oxidize indole or methimazole has been studied and can be divided into a reductive half-reaction and a followed oxidative half-reaction (Beaty and Ballou, 1981a,b; Cho *et al*., 2011). In the reductive half-reaction, flavin adenine dinucleotide (FAD) is reduced by NADPH, and the reduced FAD accepts an oxygen molecule to generate C4a-hydroperoxyflavin. The C4a-hydroperoxyflavin intermediate of Tmm is a stable form *in vivo* (Alfieri *et al*., 2008). In the oxidative half-reaction, an oxygen atom is transferred from the C4a-hydroperoxyflavin to the substrate. It has been established that in the reductive half-reaction, $NADP^+$ remains bound to Tmm, shielding the catalytic site of Tmm after FAD reduction, and promotes the stabilization of the C4a-hydroperoxyflavin intermediate (Alfieri *et al*., 2008; Orru *et al*., 2010). During the oxidative half-reaction, some studies indicated that $NADP^+$ remains bound to Tmm (Alfieri *et al*., 2008; Orru *et al*., 2010). However, later structural analysis suggested that $NADP^+$ dissociates and the substrate binds before the oxidation (Cho *et al*., 2011). Based on previous studies on indole and methimazole monooxygenation (Cho *et al*., 2011; Beaty and Ballou, 1981a,b), it is reasonable to suppose that the catalysis of TMA by Tmm can be divided into a reductive half and a followed oxidative half (Fig. 1). However, because TMA is smaller and lacks a ring structure compared with indole and methimazole, the underpinning mechanism of Tmm oxidizing TMA may be different. Till now, the structural basis for TMA oxidation is still lacking.

In this study, we cloned a *tmm* gene from *Roseovarius nubinhibens* ISM, an MRC strain isolated from surface waters of the Caribbean Sea (Gonzalez *et al*., 2003). The *tmm* gene was over-expressed in *Escherichia coli*, and the recombinant Tmm (*Rn*Tmm) was characterized. The crystal structures of *Rn*Tmm/FAD/NADPH complex, a mutant Y207S with marginal activity in complex with FAD and NADPH (the Y207S/FAD/NADPH complex), the Y207S/FAD/NADPH complex soaked with TMA and the Y207S/FAD/NADPH/methimazole complex were obtained. Structural and biochemical analyses suggest that $NADP^+$ binds to *Rn*Tmm throughout the catalytic process. In addition to reducing FAD and stabilizing the C4a-hydroperoxyflavin intermediate in the reductive half-reaction, $NADP^+$ is also involved in the oxidative half-reaction of *Rn*Tmm. Our results reveal the molecular mechanism of TMA oxidation by marine bacterial Tmms and provide novel insight into the catalytic mechanism of FMOs.

Results

Expression and characterization of Rn*Tmm*

Full-length *tmm* was amplified from *R. nubinhibens* ISM and was expressed in *E. coli* BL21(DE3) cells. The gene tmm contains 1344 nucleotides and encodes a protein of 447 residues. The optimal temperature for *Rn*Tmm enzymatic activity was ~ 30°C (Fig. 2A), and the optimal pH was ~ 8.0 (Fig. 2B). Since FMOs exhibit striking substrate promiscuity, we analyzed the substrate specificity of *Rn*Tmm (Table 1). *Rn*Tmm can oxidize TMA, methimazole, indole and dimethylamine (DMA), and TMA is the best substrate.

Overall structure of Rn*Tmm*

To study the catalytic mechanism of *Rn*Tmm to oxygenate TMA, we tried to obtain the crystal structure of *Rn*Tmm. However, X-ray analysis showed that WT *Rn*Tmm crystals suffered from severe twinning. We noticed that bacterial FMO from *Methylophaga* sp. strain SK1 (mFMO) also encountered the twinning problem (Alfieri *et al*., 2008), and that mutation of two solvent-exposed charged residues (E158A/E159A) gave mFMO

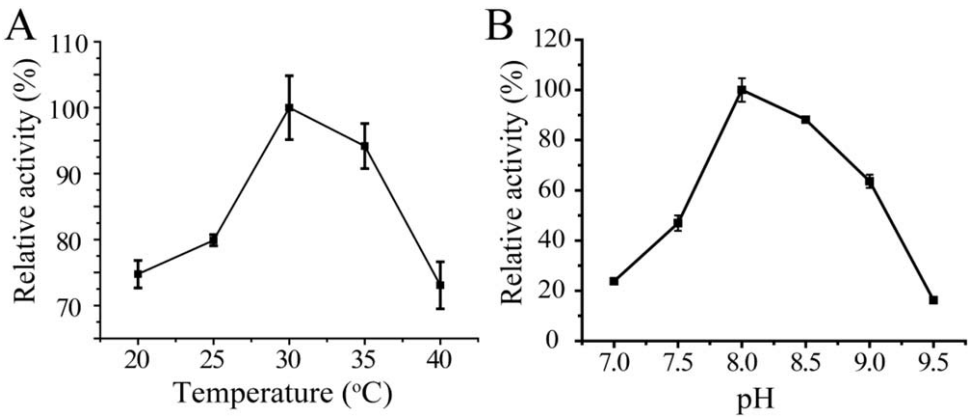

Fig. 2. Characterization of recombinant *Rn*Tmm. A. Effect of temperature on the enzymatic activity of *Rn*Tmm. B. Effect of pH on the enzymatic activity of *Rn*Tmm.

crystals free from twinning (Alfieri *et al.*, 2008). Sequence alignment indicated that *Rn*Tmm possesses E153/D154 at the equivalent position to E158/E159 of mFMO. We, therefore, generated an E153A/D154A double mutant of *Rn*Tmm. This mutation enabled *Rn*Tmm crystals free from twinning, and we obtained the 1.5 Å crystal structure of this mutant in complex with FAD and NADPH (Table 2). The biochemical properties of this mutant exhibited no substantial difference from those of WT *Rn*Tmm (Table 1), indicating that the E153A/D154A mutation had little effect on the catalytic properties of *Rn*Tmm. Thus, the E153A/D154A mutant was used to create additional mutants. For clarity, the crystal structure of E153A/D154A in complex with FAD and NADPH was simply termed as the crystal structure of WT *Rn*Tmm hereafter.

The overall structure of WT *Rn*Tmm is similar to those of other reported bacterial FMOs (Eswaramoorthy *et al.*, 2006; Alfieri *et al.*, 2008; Orru *et al.*, 2010; Cho *et al.*, 2011). WT *Rn*Tmm contains a smaller $NADP^+$ binding domain and a larger FAD binding domain, which are connected by two hinge regions (H164 to N169 and C271 to H276) (Fig. 3A). FAD molecule and $NADP^+$ molecule can be clearly observed in the structure (Fig. 3A). To obtain the crystal structure of *Rn*Tmm in complex with TMA, we constructed a mutant Y207S, which had significantly lower activity compared with that of WT *Rn*Tmm (Fig. 3B). Although our attempt to obtain the Y207S/FAD/NADPH in complex with TMA by co-crystallization was not successful, the crystal structures of Y207S/FAD/NADPH complex without ligand and of Y207S/FAD/NADPH complex soaked with TMA were determined to 1.75 Å and 1.5 Å respectively (Table 2). For briefness, the crystal structure of Y207S/FAD/NADPH complex without ligand was termed the crystal structure of Y207S and that of Y207S/FAD/NADPH complex soaked with TMA termed the crystal structure of Y207S soaking hereafter. The overall structures of Y207S and Y207S soaking are quite similar to that of WT *Rn*Tmm, with the root mean square deviation (RMSD) between WT *Rn*Tmm and Y207S of 0.42 Å, and the RMSD between WT *Rn*Tmm and Y207S soaking of 0.44 Å.

Table 1. Kinetic parameters for recombinant *Rn*Tmm with substrates.

Substrate	K_m (μM)	k_{cat} (s^{-1})
TMA	110.5 ± 14.5	0.53 ± 0.04
TMA (E153A/D154A)	85.1 ± 11.3	0.45 ± 0.03
methimazole	123.3 ± 44.6	0.22 ± 0.03
indole	244.0 ± 36.0	0.15 ± 0.01
DMA	164.9 ± 36.5	0.17 ± 0.02

Entrance for NADPH and substrates

The electron density map of *Rn*Tmm shows the location of the FAD molecule and the $NADP^+$ molecule. The FAD molecule is bound deeply in the protein (Fig. 4A). Residues N73 and T321 form hydrogen bonds with the isoalloxazine ring, the backbone carbonyl of V126 forms interaction with the adenine moiety, residues E38 and Q40 form hydrogen bonds with the ribose moiety, and residues S13, L46, W47, H63 and Q318 interact with the other parts of FAD (Fig. 4B). For the $NADP^+$ molecule, only the nicotinamide ring is located inside *Rn*Tmm, forming pi–pi stacking interaction with the isoalloxazine ring of FAD, and the other parts nest the surface of *Rn*Tmm (Fig. 4A). Residues W71, D211, and R413 form hydrogen bonds with the nicotinamide ring, residues Y173 and R229 form interactions with the adenine moiety, and residues N73, A205 and S208 interact with the other parts of $NADP^+$ (Fig. 4C).

Analysis of WT *Rn*Tmm structure indicated that the entrance is still partially solvent accessible after the $NADP^+$ molecule binds to *Rn*Tmm, and that the entrance is obviously divided into two zones, the basic

Table 2. Crystallographic data collection and refinement.

Parameters	WT *Rn*Tmm	Y207S	TMA soaking	Y207S-Methimazole
Diffraction data				
Space group	$P2_1$	$P2_1$	$P2_1$	$P2_1$
Unit cell				
a, b, c (Å)	73.5, 85.4, 79.5	72.8, 60.9, 104.7	73.0, 61.4, 104.7	60.8, 207.6, 72.5
α, β, γ (˚)	90.0, 113.0, 90.0	90.0, 93.7, 90. 0	90.0, 94.0, 90.0	90.0, 90.3, 90.0
Resolution range	50.0–1.5	50.0–1.75	50.0–1.5	50.0–2.2
(Å)	(1.55–1.50)[a]	(1.81–1.75)	(1.53–1.50)	(2.28–2.20)
Redundancy	6.2 (5.9)	6.8 (6.3)	3.6 (3.7)	3.1 (2.9)
Completeness (%)	98.8 (98.3)	98.7 (98.2)	88.2 (98.4)	93.2 (92.1)
R_{merge}[b]	0.1 (0.3)	0.1 (0.5)	0.1 (0.4)	0.2 (0.4)
$I/\sigma I$	31.1 (7.8)	14.2 (2.8)	36.8 (5.3)	10.5 (2.7)
Refinement statistics				
R-factor	0.15	0.18	0.16	0.20
Free R-factor	0.17	0.22	0.21	0.27
RMSD from ideal geometry				
Bond lengths (Å)	0.006	0.015	0.005	0.008
Bond angles (˚)	1.17	1.10	1.08	1.163
Ramachandran plot (%)				
Favored	94.9	95.4	94.4	92.7
Allowed	5.1	4.6	5.3	7.1
Outliers			0.3	0.2
Overall B-factors (Å^2)	14.1	23.6	24.3	33.07

a. Numbers in parentheses refer to data in the highest resolution shell.
b. $R_{merge} = \sum_{hkl}\sum_i |I(hkl)_i - <I(hkl)>| / \sum_{hkl}\sum_i <I(hkl)_i>$.

zone and the acidic zone (Fig. 4A). The basic zone is formed mainly by the basic side-chain of R229 and the nitrogen atoms from the main-chain of residues G204, A205 and G273; the acidic zone contains several acidic residues, such as D317, E360, E361 and D364. The $NADP^+$ molecule nests in the basic zone of the entrance by forming hydrogen bonds with *Rn*Tmm residues. Among Tmm's substrates, most contain a basic amine group, such as TMA, methimazole, *N,N* dimethylaniline and indole. Therefore, the acidic zone can attract these basic substrates, bringing an appropriate substrate into the catalytic site.

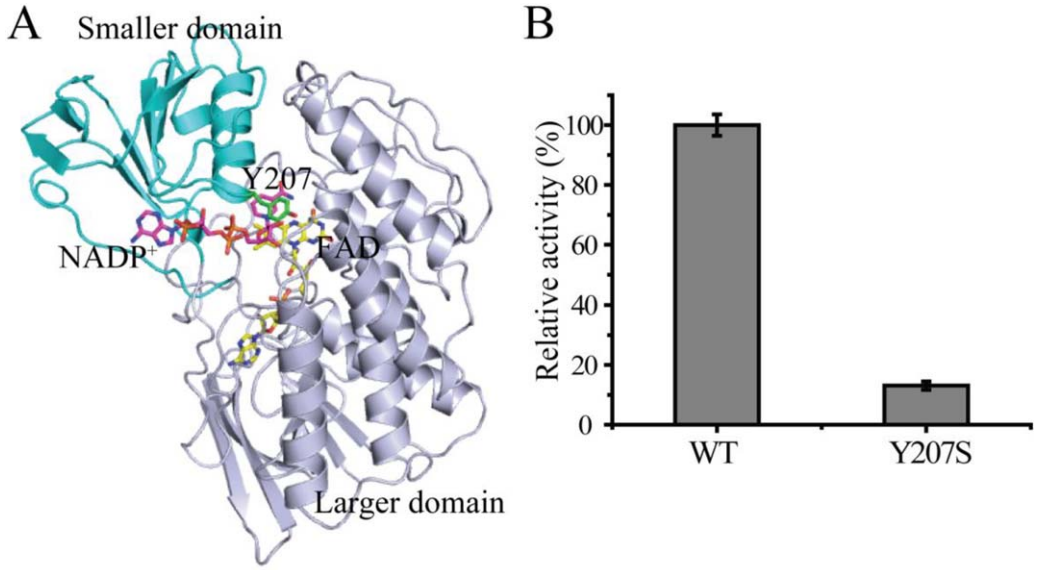

Fig. 3. Overall structure of WT *Rn*Tmm.
A. The overall structure of WT *Rn*Tmm. The *Rn*Tmm molecule contains a smaller $NADP^+$ binding domain (colored in cyan) and a larger FAD binding domain (colored in bluewhite). The $NADP^+$ molecule (colored in purple) and the FAD molecule (colored in yellow) can be clearly identified in the structure. Residue Y207 is colored in green.
B. The effect of mutation Y207S on the enzymatic activity of *Rn*Tmm. The activity of WT *Rn*Tmm was defined as 100%.

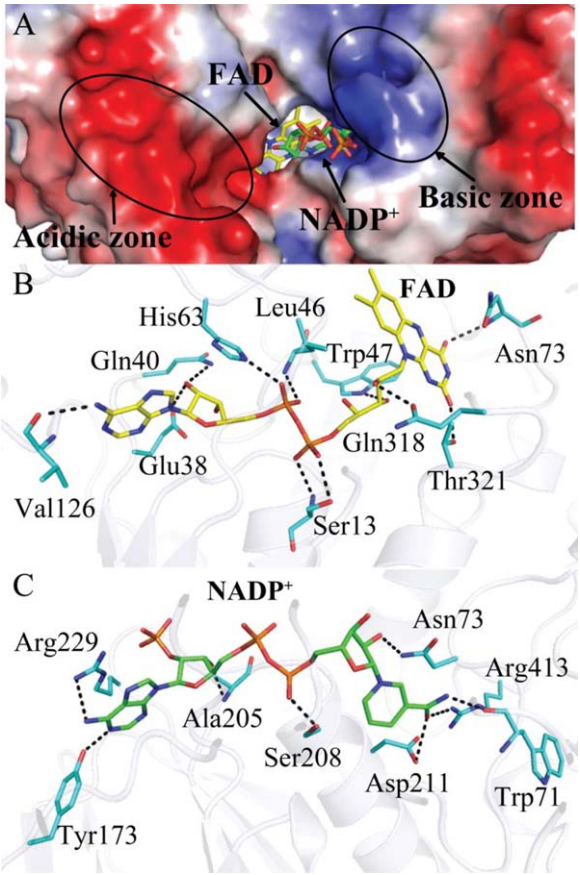

Fig. 4. The binding of the FAD and NADP$^+$ molecules of *Rn*Tmm. The FAD molecule is colored in yellow, the NADP$^+$ molecule is colored in blue, and the *Rn*Tmm residues are colored in cyan.
A. Electrostatic surface of the crystal structure of *Rn*Tmm. The FAD molecule is buried in *Rn*Tmm, while only the nicotinamide ring of NADP$^+$ is inserted into *Rn*Tmm. The entrance for substrates can be divided into two zones, the basic zone and the acidic zone.
B. Interactions between *Rn*Tmm residues and FAD. The possible hydrogen bonds are represented by dashed lines.
C. Interactions between *Rn*Tmm residues and NADP$^+$. The possible hydrogen bonds are represented by dashed lines.

Conformational change of NADP$^+$ molecule in the oxidative half-reaction

A quaternary complex containing Y207S, FAD, NADP$^+$ and TMA was expected in the crystal structure of Y207S soaking; however, not explicit electron density of TMA was identified during structural refinement. By superimposing the catalytic site structures of WT *Rn*Tmm, Y207S and Y207S that was soaked with TMA, we found that the FAD molecules are perfectly superimposed among these three structures (Fig. 5A). Interestingly, the NADP$^+$ molecules are perfectly superimposed in WT *Rn*Tmm and Y207S structures, but the Y207S that had been soaked with TMA exhibits a conformational change (Fig. 5B). In addition, the electron density map for the nicotinamide

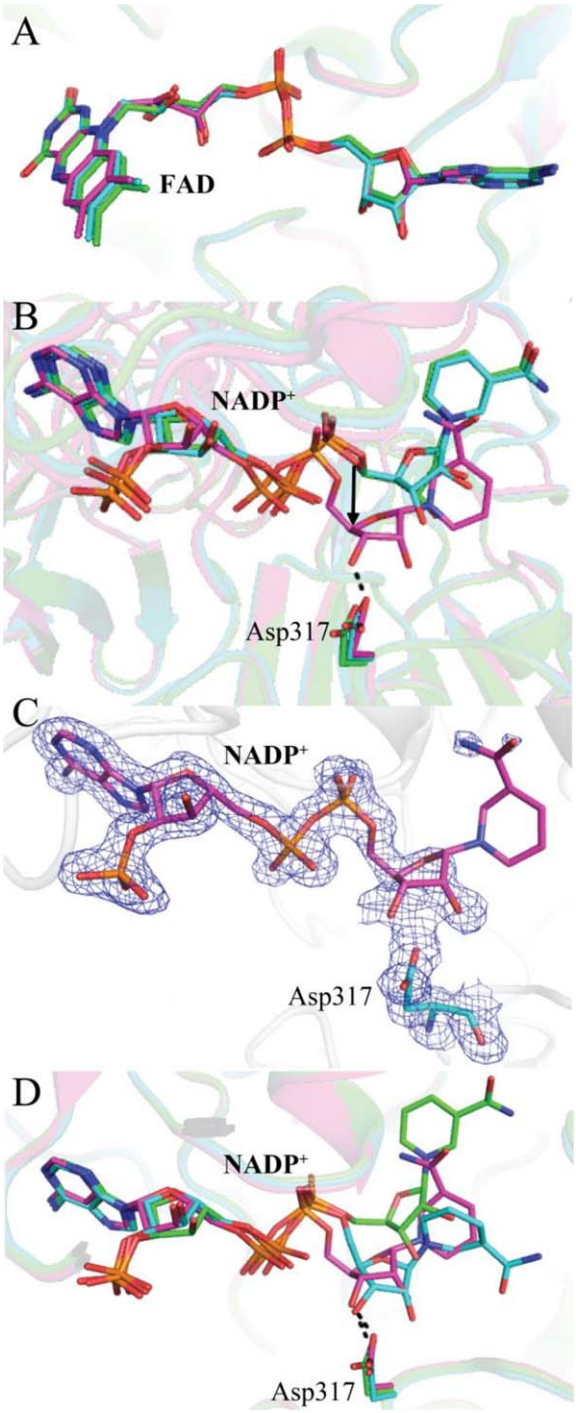

Fig. 5. Analysis of the conformational change of NADP$^+$.
A. The conformation of FAD in the crystal structures of WT *Rn*Tmm (colored in green), Y207S (colored in cyan) and Y207S soaking (colored in purple).
B. The conformation of NADP$^+$ in the crystal structures of WT *Rn*Tmm, Y207S and Y207S soaking. The colors are same to (A). The conformational change of NADP$^+$ is indicated by black arrow.
C. The $2F_o$–F_c densities for NADP$^+$ and D317 from the structure of Y207S soaking are contoured in blue at 1.5σ.
D. The conformation of NADP$^+$ in the crystal structures of Y207S (colored in green), Y207S soaking (colored in purple) and Y207S-methimazole (colored in cyan).

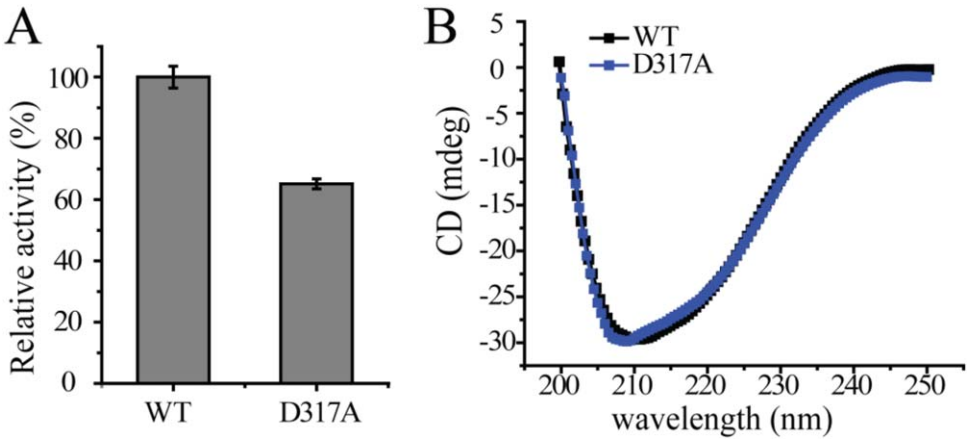

Fig. 6. Analysis of the important role of the residue D317.
A. Enzymatic activities of the mutant D317A and WT *Rn*Tmm. The activity of WT *Rn*Tmm was defined as 100%.
B. Circular-dichroism spectra of the mutant D317A and WT *Rn*Tmm.

ring of $NADP^+$ in the structure of Y207S that had been soaked with TMA is rather poor under the 1.5 Å resolution, whereas the electron density map for the other parts of $NADP^+$ is clear (Fig. 5C), indicating that the nicotinamide ring of $NADP^+$ becomes mobile during soaking. Notably, the electron density map strongly indicates an interaction between $NADP^+$ and D317 in Y207S soaking (Fig. 5C). Compared with those in WT *Rn*Tmm and Y207S, the ribose ring connecting to the nicotinamide ring of $NADP^+$ in Y207S soaking moves approximate 2.7 Å toward D317, and forms a hydrogen bond with the side-chain of D317 (Fig. 5B). Because D317 is one of the residues constituting the acidic zone of the substrate entrance, the formation of the hydrogen bond between $NADP^+$ and D317 can "shut off" the substrate entrance of *Rn*Tmm and make the catalytic site solvent inaccessible, thereby forming a relatively enclosed micro-environment for the catalytic reaction. In addition, a mutation of D317 to alanine decreased the activity of *Rn*Tmm significantly (Fig. 6), further indicating the importance of the interaction between $NADP^+$ and D317 in the catalytic cycle of *Rn*Tmm.

Among substrates *Rn*Tmm can catalyze, TMA and DMA are relatively small molecules, whereas methimazole and indole both possess a ring structure. To find out whether substrates possessing a ring structure also induce a conformational change of $NADP^+$, we solved the crystal structure of Y207S/FAD/NADPH/methimazole complex (Y207S-methimazole). The overall structure of Y207S-methimazole is similar to that of WT *Rn*Tmm, with the RMSD of 0.22 Å between these two structures. In the crystal structure of Y207S-methimazole, electron density map indicates that the $NADP^+$ molecule also undergoes a conformational change during methimazole soaking, and that the ribose ring connecting to the nicotinamide ring of $NADP^+$ also forms a hydrogen bond with D317 (Fig. 5D). These results indicate that *Rn*Tmm adopts similar strategies to catalyze different substrates.

In addition to "shut off" the substrate entrance, the $NADP^+$ bending in Y207S soaking also breaks the interactions between the nicotinamide ring of $NADP^+$ and the isoalloxazine ring of FAD (Fig. 7). In the structures

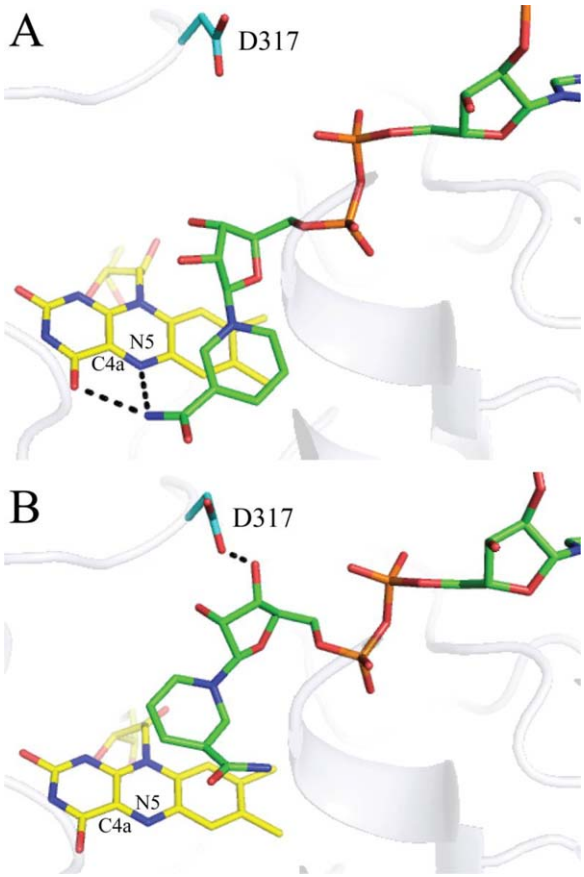

Fig. 7. Interactions between $NADP^+$ and FAD. The FAD molecule is colored in yellow, the $NADP^+$ molecule in green, and residue D317 in cyan. The possible hydrogen bonds are represented by dashed lines.
A. The conformation of $NADP^+$ and FAD in the structure of WT *Rn*Tmm.
B. The conformation of $NADP^+$ and FAD in the structure of Y207S soaking.

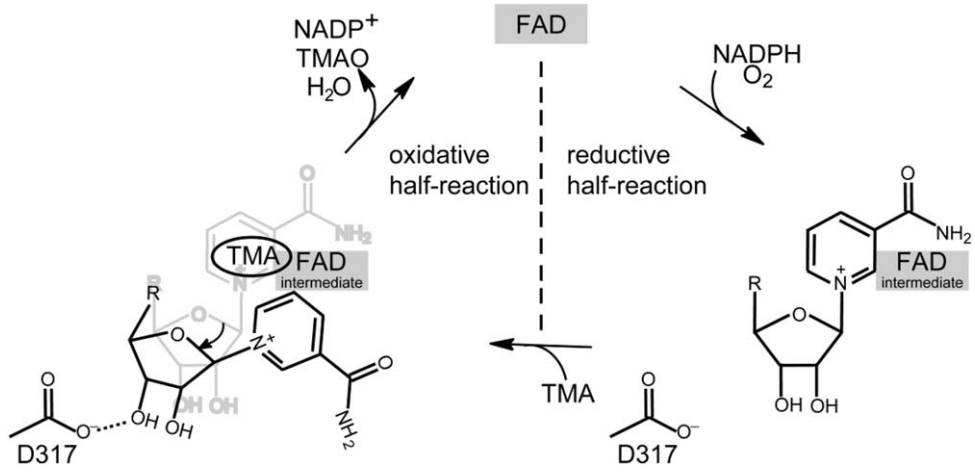

Fig. 8. The catalytic cycle of *Rn*Tmm to oxidize TMA into TMAO. In the reductive half-reaction, the C4a-hydroperoxyflavin intermediate is formed. The $NADP^+$ molecule remains in the active site, shielding the C4a-hydroperoxyflavin intermediate from solvent attack. Once TMA comes into the catalytic pocket, the $NADP^+$ undergoes a conformational change to form a hydrogen bond with D317, shutting off the entrance and exposing the C4a-hydroperoxyflavin to oxidize TMA. After the reaction, $NADP^+$ and the produced TMAO are released, and the FAD is regenerated. FAD intermediate indicates the C4a-hydroperoxyflavin.

of WT *Rn*Tmm and Y207S, the nicotinamide ring of $NADP^+$ forms stacking interactions with the isoalloxazine ring of FAD, and the nitrogen atom of the nicotinamide ring of $NADP^+$ forms hydrogen bonds with the nitrogen atom or the oxygen atom of the isoalloxazine ring of FAD (Fig. 7A). The interactions between the two rings are essential for stabilization of the C4a-hydroperoxyflavin intermediate by $NADP^+$ (Alfieri *et al.*, 2008; Orru *et al.*, 2010). In the structure of Y207S soaking, the electron density of the nicotinamide ring is poor (Fig. 5C), suggesting that there may be no direct interactions between $NADP^+$ and FAD (Fig. 7B). However, the $NADP^+$ does seem to close off the entrance to protect the C4a-hydroperoxyflavin.

The catalytic cycle of Rn*Tmm with TMA as a substrate*

Based on previous studies on the reductive half-reaction of Tmm catalysis (Alfieri *et al.*, 2008; Orru *et al.*, 2010) and our results on the oxidative half-reaction, we propose a relatively complete catalytic cycle of *Rn*Tmm with TMA as a substrate (Fig. 8). In the reductive half-reaction, NADPH reduces FAD and the C4a-hydroperoxyflavin intermediate forms. It is believed that Tmm spends most of the time in this intermediate state *in vivo* (Alfieri *et al.*, 2008). In the intermediate state, the $NADP^+$ molecule nests the basic zone of the entrance for substrates, and the catalytic pocket of *Rn*Tmm is still partially solvent accessible. The nicotinamide ring of $NADP^+$ inserted in *Rn*Tmm protects the C4a-hydroperoxyflavin intermediate from solvent attack (Beaty and Ballou, 1981b). The acidic zone of *Rn*Tmm attracts a TMA molecule and directs it into the catalytic pocket. Once TMA enters the catalytic pocket, it occupies the catalytic site and makes $NADP^+$ bend to start the oxidative half-reaction. $NADP^+$ bending would result in two consequences: Firstly, the ribose ring connecting to the nicotinamide ring of $NADP^+$ forms a hydrogen bond with D317, shutting off the substrate entrance and promoting a protected micro-environment for the catalytic reaction; Secondly, the nicotinamide ring of $NADP^+$ that protects the C4a-hydroperoxyflavin shifts, exposing the C4a-hydroperoxyflavin to the substrate for catalysis (Fig. 8). After the oxygenation, the C4a-position of the FAD bears an —OH group, which loses water, $NADP^+$ and TMAO to regenerate the oxidized FAD. In the next catalytic cycle, an NADPH molecule re-binds to *Rn*Tmm, reduces the FAD, and shields the C4a-hydroperoxyflavin intermediate, enabling *Rn*Tmm to get ready for the oxygenation of the next substrate.

Universality of the catalytic cycle of Rn*Tmm to oxidize TMA into TMAO in bacteria*

The *tmm* gene is widespread in many marine bacteria, especially in MRC and the SAR11 clade. Most bacterial strains containing *tmm* homologs can grow on TMA as a sole nitrogen source (Chen *et al.*, 2011), implying the importance of these bacterial strains in metabolizing TMA in the ocean. In addition, many soil bacteria also contain *tmm* homologs, for example, *Rhizobium* and *Mesorhizobium*. To analyze the universality of the catalytic mechanism of *Rn*Tmm to oxidize TMA into TMAO in bacteria, we performed sequence alignment of

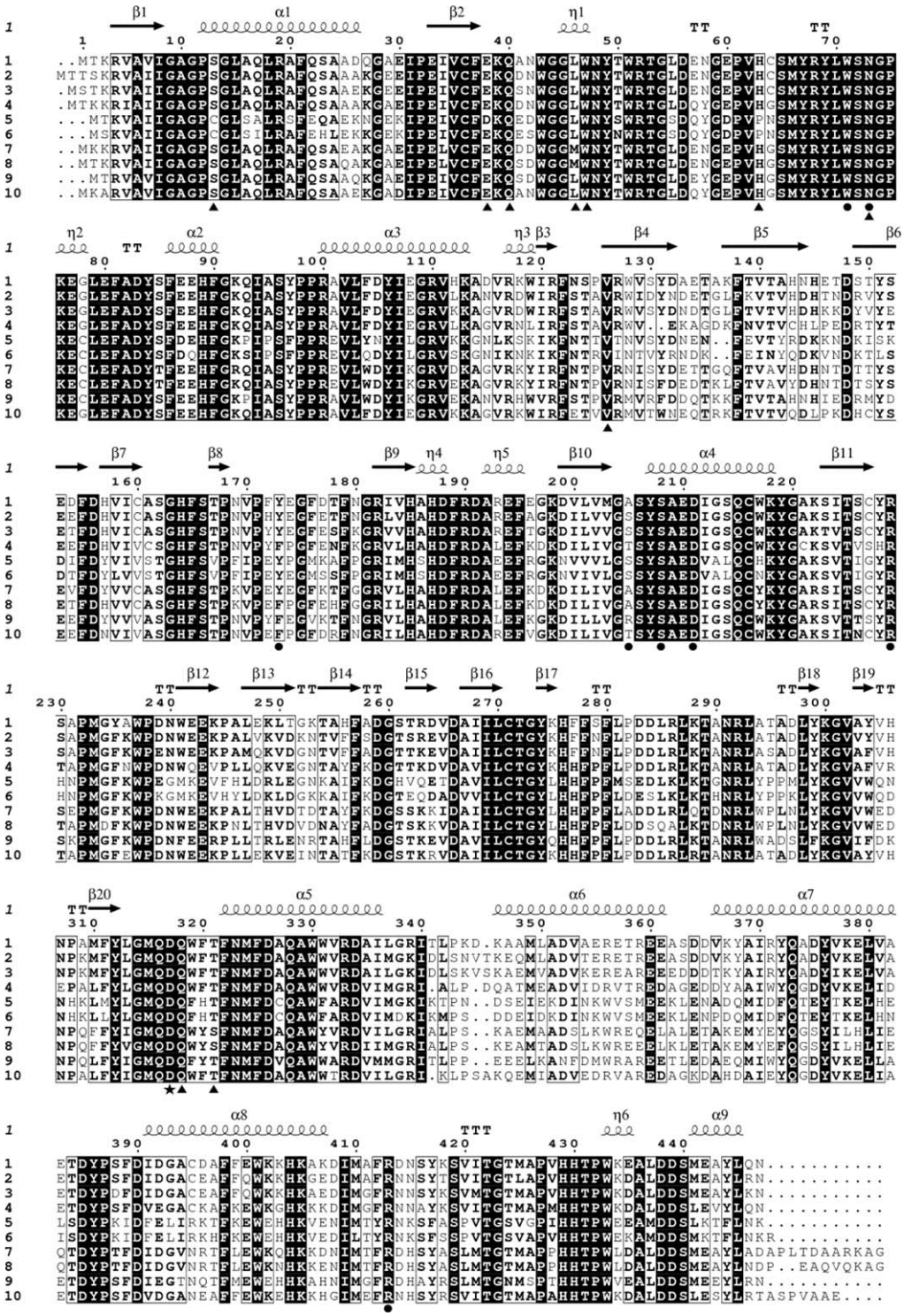

Fig. 9. Sequence alignment of bacterial Tmm proteins. Black dots indicate residues involved in NADPH binding, black triangles indicate residues involved in FAD binding, and residue D317 is marked by a black star. Sequences 1–8 are Tmm's from marine bacteria, including 1–4 from MRC and 5–6 from the SAR11 clade. Sequences 9–10 are Tmm's from soil bacteria. 1, *Roseovarius nubinhibens* ISM, EAP78254.1; 2, *Ruegeria pomeroyi* DSS3, WP_011047288.1; 3, *Roseobacter denitrificans*, WP_044032905.1; 4, *Roseovarius* sp. 217, WP_009818593.1; 5, *Pelagibacter ubique* HTCC1002, WP_006997992.1; 6, *Pelagibacter ubique* HTCC7211, WP_008544347.1; 7, *Marinobacterium stanieri*, WP_029511274.1; 8, *Marinobacterium litorale*, WP_027855190.1; 9, *Rhizobium leguminosarum*, WP_025397603.1; and 10, *Mesorhizobium* sp. 1M-11, WP_054310147.1. The alignment was done with ClustalW (Chenna *et al.*, 2003) and ESPript (Robert and Gouet, 2014).

bacterial Tmms. The result showed that residue D317 and most residues involved in binding FAD and $NADP^+$ in *Rn*Tmm are highly conserved in Tmms from both marine bacteria and soil bacteria (Fig. 9). This indicates that the proposed catalytic cycle of *Rn*Tmm to oxidize TMA into TMAO is likely adopted by most, if not all, bacterial Tmms.

Discussion

Many studies on the catalytic mechanisms of both eukaryotic and bacterial FMOs have been reported and it is regarded as a general characteristic of FMOs that the coenzyme $NADP^+$ remains bound to the enzyme throughout catalysis (Van Berkel *et al*., 2006; Alfieri *et al*., 2008; Orru *et al*., 2010; Crozier-Reabe and Moran, 2012). However, a structural study by Cho *et al*. suggested that for the catalysis of indole by Tmm from *Methylophaga aminosulfidovorans* MP^T, indole competes with $NADP^+$ for binding to the catalytic site and $NADP^+$ is released before the oxidative half-reaction (Cho *et al*., 2011). After the departure of $NADP^+$, the C4a-hydroperoxyflavin intermediate might be transitorily stabilized by residues of the enzyme (Cho *et al*., 2011). Here, our data showed that TMA only competes the nicotinamide ring of $NADP^+$, and the $NADP^+$ molecule remains bound to Tmm until the catalytic reaction finishes, which is in accordance with the general characteristics of FMOs (Van Berkel *et al*., 2006; Crozier-Reabe and Moran, 2012). This is the first structural evidence that $NADP^+$ binds to Tmm throughout the catalysis of TMA.

In addition to reducing FAD, it has been reported that NADP(H) also exhibited a moonlighting activity to protect the C4a-hydroperoxyflavin intermediate during the reductive half-reaction of the catalysis (Alfieri *et al*., 2008; Orru *et al*., 2010). Although studies indicated that $NADP^+$ binds to FMOs throughout the catalysis (Van Berkel *et al*., 2006; Alfieri *et al*., 2008; Orru *et al*., 2010; Crozier-Reabe and Moran, 2012), the role of $NADP^+$ in the oxidative half-reaction is not explicit yet. Our results indicate that the $NADP^+$ molecule undergoes a conformational change in the oxidative half-reaction, which exposes the catalytic C4a-hydroperoxyflavin to TMA, and promotes a protected micro-environment for the catalytic reaction of Tmm by forming a hydrogen bond with a conserved aspartic acid residue. Therefore, in addition to functioning in the reductive half-reaction, NADPH/$NADP^+$ also plays an important role in the oxidative half-reaction of Tmm for TMA oxidation. $NADP^+$ bending was also identified in Baeyer-Villiger monooxygenases (BVMOs) (Yachnin *et al*., 2012), another subclass of the class B flavoprotein monooxygenases (Riebel *et al*., 2014). For BVMOs, intramolecular hydrogen bonds are important in stabilizing the rotated conformation of $NADP^+$ (Yachnin *et al*., 2012). Here for FMOs, we highlight the importance of interactions between $NADP^+$ and Tmm. In both cases, $NADP^+$ bending exposes the catalytic site and promotes the oxidative reaction (Yachnin *et al*., 2012). Therefore, our study on FMOs should enrich our understanding of the catalytic cycle of flavoprotein monooxygenases.

Structural analysis demonstrated that there is no direct interaction between the substrate and the residues of Tmm (Eswaramoorthy *et al*., 2006; Cho *et al*., 2011). Substrates containing a ring structure, such as indole and methimazole, can form stacking interactions with the isoalloxazine ring of FAD (Eswaramoorthy *et al*., 2006; Cho *et al*., 2011). Because TMA does not possess a ring structure, there may be no effective interaction to stabilize its conformation when TMA enters the catalytic pocket, and the positive charge on TMA probably repels the positive charge on the pyridinium ring of $NADP^+$ to drive the movement of the nicotinamide during the reaction. In the catalytic cycle of Tmm, when TMA enters the catalytic site, it should be directed to the C4a-hydroperoxyflavin, triggering the oxidative half-reaction. Because TMA molecule cannot form stacking interactions with FAD, we suggest that the catalytic reaction of Tmm proceeds quickly, and a prolonged steady-conformation of TMA is not necessary. This may be the reason why we have observed the conformational change of $NADP^+$, but cannot identify the location of TMA in the structure of Y207S soaked with TMA. The aromatic ring of Y207 residue forms a pi-pi stacking with the isoalloxazine ring of FAD in the Tmm without NADPH (Orru *et al*., 2010; Cho *et al*., 2011). When NADPH binds to the catalytic site, it competes for the isoalloxazine ring and frees Y207 (Orru *et al*., 2010; Cho *et al*., 2011). Thus, the isoalloxazine ring moves between the aromatic ring of Y207 and the nicotinamide ring of $NADP^+$, and Y207 plays a role in releasing $NADP^+$ after each catalytic cycle during TMA oxidation.

In conclusion, this study illustrated the catalytic cycle of TMA oxidation by marine *Rn*Tmm and showed the first structural evidence of $NADP^+$ binding to a Tmm throughout the catalytic reaction and its involvement in the oxidative half-reaction by a conformational bending. The proposed mechanism of TMA oxidation by *Rn*Tmm may have universal significance among bacteria containing Tmm. Our results provide novel insights into the catalytic mechanism of FMOs and promote a better understanding of TMA-involved marine carbon and nitrogen cycling.

Experimental procedures

Bacterial strains and growth conditions

R. nubinhibens ISM was purchased from the Leibniz Institute DSMZ-German Collection of Microorganisms and Cell Cultures and was cultured in the 974 medium at 30°C for 2 days according to the provided protocol (http://www.dsmz.de/). *E. coli* strains DH5α and BL21 (DE3) were grown in Lysogeny Broth (LB) medium at 37°C.

Gene cloning, point mutation and protein expression and purification

The *tmm* gene was amplified from the genomic DNA of *R. nubinhibens* ISM using PCR and was subcloned into the pET22b (Novagen) vector with a C-terminal His tag. All of the point mutations (E153A/D154A, Y207S and D317A) in *Rn*Tmm were introduced using PCR-based methods and were verified by DNA sequencing. Y207S and D317A were constructed base on mutant E153A/D154A. The *Rn*Tmm protein and all of its mutants were expressed in *E. coli* strain BL21 (DE3). The cells were cultured at 37°C in LB medium to an OD_{600} of 0.8–1.0 and then induced at 20°C for 16 h with 0.5 mM isopropyl β-D-1-thiogalactopyranoside (IPTG). The proteins were purified first with Ni^{2+}-NTA resin (Qiagen) and then fractionated by gel filtration on a Superdex-200 column (GE Healthcare).

Enzyme assays

The enzymatic properties of *Rn*Tmm were measured by following the decrease of absorbance at 340 nm ($\varepsilon_{340} = 6.22$ mM^{-1} cm^{-1} for NADPH) (Alfieri *et al.*, 2008). The reaction mixture contains 1 μM *Rn*Tmm, 0.25 mM NADPH and 1 mM TMA. For the measurement of K_m of *Rn*Tmm, substrate (TMA, methimazole, indole or DMA) of different concentrations was added into the reaction system containing 1 μM *Rn*Tmm and 0.25 mM NADPH. The optimal pH and the optimal temperature of *Rn*Tmm were determined using TMA as the substrate. For measurement of the optimal temperature of *Rn*Tmm, a buffer containing 10 mM Tris-HCl (pH 8.0) and 100 mM NaCl was pre-incubated at different temperatures for 30 min, and then 1 μM *Rn*Tmm, 0.25 mM NADPH and 1 mM TMA were added into the buffer and the mixture was incubated at different temperatures for 3 min before detection by V550 UV/VIS spectrophotometer (Jasco). The optimal pH of *Rn*Tmm was measured using Britton-Robinson buffer over a pH range from 7.0 to 9.5. Britton-Robinson buffer is a mixture of 0.04 M H_3BO_3, 0.04 M H_3PO_4 and 0.04 M CH_3COOH (Barek *et al.*, 1999).

The enzymatic activities of *Rn*Tmm mutants were determined by detecting the fluorescence of indoxyl on a FP-6500 spectrofluorometer (Jasco) (Woo *et al.*, 2000). The reaction mixture contained 2 μM *Rn*Tmm or a mutant, 0.15 mM NADPH and 0.15 mM indole. The mixture was incubated for 10 min before detection. Fluorescence spectra were collected from 450 to 490 nm at a scan speed of 1000 nm min^{-1} with the excitation wavelength of 365 nm (Woo *et al.*, 2000).

Crystallization and data collection

The purified *Rn*Tmm protein was concentrated to approximately 10 mg ml^{-1} in 10 mM Tris-HCl (pH 8.0) and 100 mM NaCl. To obtain crystals of WT *Rn*Tmm, NADPH was added into the protein solution to a final concentration of 5 mM before crystallization. Initial crystallization trials for WT *Rn*Tmm were performed at 20°C using the sitting drop vapor diffusion method. Diffraction-quality crystals of WT *Rn*Tmm were obtained in hanging drops containing 0.2 M magnesium acetate tetrahydrate, 0.1 M sodium cacodylate trihydrate (pH 6.5) and 20% (w/v) polyethylene glycol (PEG) 8000 at 20°C after 2-weeks incubation.

Diffraction-quality crystals of Y207S were obtained in hanging drops containing 0.2 M sodium acetate, 0.1 M Bis-Tris propane (pH 6.5) and 20% (w/v) PEG 3350 at 20°C. The crystals of Y207S soaking were obtained using crystals of Y207S soaked with 15 mM TMA for 15 min. The crystals of Y207S-methimazole were obtained using crystals of Y207S soaked with 15 mM methimazole for 15 min. X-ray diffraction data were collected on the BL19U1 beamline at the Shanghai Synchrotron Radiation Facility. The initial diffraction data sets were processed by the HKL3000 program (Minor *et al.*, 2006).

Structure determination and refinement

The crystals of WT *Rn*Tmm, Y207S, Y207S soaking and Y207S-methimazole all belong to the $P2_1$ space group. The crystal structure of WT *Rn*Tmm was determined by molecular replacement using the CCP4 program Phaser (Potterton *et al.*, 2003) with the crystal structure of bacterial FMO (PDB code: 2XVE) as the search model. The structures of Y207S, Y207S soaking and Y207S-methimazole were determined using WT *Rn*Tmm as the search model. The refinements of these structures were performed using Coot (Emsley and Cowtan, 2004) and *Phenix* (Adams *et al.*, 2002). All of the structure figures were made using the program PyMOL (http://www.pymol.org/).

Circular-dichroism (CD) spectroscopic assays

WT *Rn*Tmm and its mutant were subjected to CD spectroscopic assays at 25°C on a J-810 spectropolarimeter (Jasco). CD spectra of the samples at a final concentration of approximately 10 μM were collected from 250 to 200 nm at a scan speed of 500 nm min^{-1} with a band width of 2 nm. All of the samples were in the buffer containing 10 mM Tris-HCl (pH 8.0) and 100 mM NaCl.

Accession numbers

The structures of WT *Rn*Tmm, Y207S, Y207S soaking and Y207S- methimazole have been deposited in the Protein Data Bank (PDB) under the accession codes 5IPY, 5IQ1, 5IQ4 and 5GSN respectively.

Acknowledgements

We thank the staff of BL19U1 beamline at National Center for Protein Sciences Shanghai and Shanghai Synchrotron Radiation Facility, Shanghai, People's Republic of China, for assistance during data collection. This work was supported by the National Science Foundation of China (31290231, 31630012), the Program of Shandong for Taishan Scholars (TS20090803), the Hi-Tech Research and Development program of China (2012AA092105) and the National Postdoctoral Program for Innovative Talents (BX201600095).

Conflict of Interest

The authors declare that they have no conflicts of interest with the contents of this article.

References

Adams, P.D., Grosse-Kunstleve, R.W., Hung, L.W., Ioerger, T.R., McCoy, A.J., Moriarty, N.W., *et al.* (2002) PHENIX: building new software for automated crystallographic structure determination. *Acta Crystallogr D Biol Crystallogr* **58**: 1948–1954.

Alfieri, A., Malito, E., Orru, R., Fraaije, M.W., and Mattevi, A. (2008) Revealing the moonlighting role of NADP in the structure of a flavin-containing monooxygenase. *Proc Natl Acad Sci U S A* **105**: 6572–6577.

Arata, H., Shimizu, M., and Takamiya, K. (1992) Purification and properties of trimethylamine *N*-oxide reductase from aerobic photosynthetic bacterium *Roseobacter denitrificans*. *J Biochem* **112**: 470–475.

Barek, J., Pumera, M., Muck, A., Kadeřábková, M., and Zima, J. (1999) Polarographic and voltammetric determination of selected nitrated polycyclic aromatic hydrocarbons. *Anal Chim Acta* **393**: 141–146.

Beaty, N.B., and Ballou, D.P. (1981a) The oxidative half-reaction of liver microsomal FAD-containing monooxygenase. *J Biol Chem* **256**: 4619–4625.

Beaty, N.B., and Ballou, D.P. (1981b) The reductive half-reaction of liver microsomal FAD-containing monooxygenase. *J Biol Chem* **256**: 4611–4618.

Buchan, A., Gonzalez, J.M., and Moran, M.A. (2005) Overview of the marine roseobacter lineage. *Appl Environ Microbiol* **71**: 5665–5677.

Carpenter, L.J., Archer, S.D., and Beale, R. (2012) Ocean-atmosphere trace gas exchange. *Chem Soc Rev* **41**: 6473–6506.

Cashman, J.R. (1995) Structural and catalytic properties of the mammalian flavin-containing monooxygenase. *Chem Res Toxicol* **8**: 166–181.

Cashman, J.R., and Zhang, J. (2006) Human flavin-containing monooxygenases. *Annu Rev Pharmacol Toxicol* **46**: 65–100.

Chen, Y. (2012) Comparative genomics of methylated amine utilization by marine *Roseobacter* clade bacteria and development of functional gene markers (tmm, gmaS). *Environ Microbiol* **14**: 2308–2322.

Chen, Y., Patel, N.A., Crombie, A., Scrivens, J.H., and Murrell, J.C. (2011) Bacterial flavin-containing monooxygenase is trimethylamine monooxygenase. *Proc Natl Acad Sci U S A* **108**: 17791–17796.

Chenna, R., Sugawara, H., Koike, T., Lopez, R., Gibson, T.J., Higgins, D.G., and Thompson, J.D. (2003) Multiple sequence alignment with the Clustal series of programs. *Nucleic Acids Res* **31**: 3497–3500.

Cho, H.J., Cho, H.Y., Kim, K.J., Kim, M.H., Kim, S.W., and Kang, B.S. (2011) Structural and functional analysis of bacterial flavin-containing monooxygenase reveals its ping-pong-type reaction mechanism. *J Struct Biol* **175**: 39–48.

Choi, H.S., Kim, J.K., Cho, E.H., Kim, Y.C., Kim, J.I., and Kim, S.W. (2003) A novel flavin-containing monooxygenase from *Methylophaga* sp strain SK1 and its indigo synthesis in *Escherichia coli*. *Biochem Biophys Res Commun* **306**: 930–936.

Crozier-Reabe, K., and Moran, G.R. (2012) Form follows function: structural and catalytic variation in the class a flavoprotein monooxygenases. *Int J Mol Sci* **13**: 15601–15639.

Emsley, P., and Cowtan, K. (2004) Coot: model-building tools for molecular graphics. *Acta Crystallogr D Biol Crystallogr* **60**: 2126–2132.

Eswaramoorthy, S., Bonanno, J.B., Burley, S.K., and Swaminathan, S. (2006) Mechanism of action of a flavin-containing monooxygenase. *Proc Natl Acad Sci U S A* **103**: 9832–9837.

Gibb, S.W., and Hatton, A.D. (2004) The occurrence and distribution of trimethylamine-*N*-oxide in Antarctic coastal waters. *Mar Chem* **91**: 65–75.

Gon, S., Giudici-Orticoni, M.T., Mejean, V., and Iobbi-Nivol, C. (2001) Electron transfer and binding of the c-type cytochrome TorC to the trimethylamine N-oxide reductase in *Escherichia coli*. *J Biol Chem* **276**: 11545–11551.

Gonzalez, J.M., Covert, J.S., Whitman, W.B., Henriksen, J.R., Mayer, F., Scharf, B., *et al.* (2003) *Silicibacter pomeroyi* sp. nov. and *Roseovarius nubinhibens* sp. nov., dimethylsulfoniopropionate-demethylating bacteria from marine environments. *Int J Syst Evol Microbiol* **53**: 1261–1269.

Koch, M., Vorwerk, S., Masur, C., Sharifi-Sirchi, G., Olivieri, N., and Schlaich, N.L. (2006) A role for a flavin-containing mono-oxygenase in resistance against microbial pathogens in *Arabidopsis*. *Plant J* **47**: 629–639.

Krueger, S.K., and Williams, D.E. (2005) Mammalian flavin-containing monooxygenases: structure/function, genetic polymorphisms and role in drug metabolism. *Pharmacol Ther* **106**: 357–387.

Ma, J.Q., Pazos, I.M., and Gai, F. (2014) Microscopic insights into the protein-stabilizing effect of trimethylamine *N*-oxide (TMAO). *Proc Natl Acad Sci U S A* **111**: 8476–8481.

Minor, W., Cymborowski, M., Otwinowski, Z., and Chruszcz, M. (2006) HKL-3000: the integration of data reduction and structure solution–from diffraction images to an initial model in minutes. *Acta Crystallogr D Biol Crystallogr* **62**: 859–866.

Mitchell, S.C., and Smith, R.L. (2001) Trimethylaminuria: the fish malodor syndrome. *Drug Metab Dispos* **29**: 517–521.

Morris, R.M., Rappe, M.S., Connon, S.A., Vergin, K.L., Siebold, W.A., Carlson, C.A., and Giovannoni, S.J. (2002) SAR11 clade dominates ocean surface bacterioplankton communities. *Nature* **420**: 806–810.

Orru, R., Pazmino, D.E.T., Fraaije, M.W., and Mattevi, A. (2010) Joint functions of protein residues and NADP(H) in oxygen activation by flavin-containing monooxygenase. *J Biol Chem* **285**: 35021–35028.

Potterton, E., Briggs, P., Turkenburg, M., and Dodson, E. (2003) A graphical user interface to the CCP4 program suite. *Acta Crystallogr D Biol Crystallogr* **59**: 1131–1137.

Quinn, P.K., Charlson, R.J., and Bates, T.S. (1988) Simultaneous observations of ammonia in the atmosphere and ocean. *Nature* **335**: 336–338.

Riebel, A., Fink, M.J., Mihovilovic, M.D., and Fraaije, M.W. (2014) Type II flavin-containing monooxygenases: a new class of biocatalysts that harbors baeyer–villiger monooxygenases with a relaxed coenzyme specificity. *ChemCatChem* **6**: 1112–1117.

Robert, X., and Gouet, P. (2014) Deciphering key features in protein structures with the new ENDscript server. *Nucleic Acids Res* **42**: W320–W324.

Rusch, D.B., Halpern, A., Sutton, L.G., Heidelberg, K., Williamson, B., Yooseph, S., *et al* (2007) The Sorcerer II Global Ocean Sampling expedition: northwest Atlantic through eastern tropical Pacific. *PLoS Biol* **5**: e77.

Schlaich, N.L. (2007) Flavin-containing monooxygenases in plants: looking beyond detox. *Trends Plant Sci* **12**: 412–418.

Seibel, B.A., and Walsh, P.J. (2002) Trimethylamine oxide accumulation in marine animals: relationship to acylglycerol storage. *J Exp Biol* **205**: 297–306.

Suh, J.K., and Robertus, J.D. (2000) Yeast flavin-containing monooxygenase is induced by the unfolded protein response. *Proc Natl Acad Sci U S A* **97**: 121–126.

Suh, J.K., Poulsen, L.L., Ziegler, D.M., and Robertus, J.D. (1999) Yeast flavin-containing monooxygenase generates oxidizing equivalents that control protein folding in the endoplasmic reticulum. *Proc Natl Acad Sci U S A* **96**: 2687–2691.

Van Berkel, W.J., Kamerbeek, N.M., and Fraaije, M.W. (2006) Flavoprotein monooxygenases, a diverse class of oxidative biocatalysts. *J Biotechnol* **124**: 670–689.

Woo, H., Sanseverino, J., Cox, C.D., Robinson, K.G., and Sayler, G.S. (2000) The measurement of toluene dioxygenase activity in biofilm culture of Pseudomonas putida F1. *J Microbiol Methods* **40**: 181–191.

Yachnin, B.J., Sprules, T., McEvoy, M.B., Lau, P.C., and Berghuis, A.M. (2012) The substrate-bound crystal structure of a Baeyer-Villiger monooxygenase exhibits a Criegee-like conformation. *J Am Chem Soc* **134**: 7788–7795.

Yancey, P.H., Gerringer, M.E., Drazen, J.C., Rowden, A.A., and Jamieson, A. (2014) Marine fish may be biochemically constrained from inhabiting the deepest ocean depths. *Proc Natl Acad Sci U S A* **111**: 4461–4465.

Zhou, J., and Shephard, E.A. (2006) Mutation, polymorphism and perspectives for the future of human flavin-containing monooxygenase 3. *Mutat Res* **612**: 165–171.

